Tetrahedron 72 (2016) 7796–7804

Contents lists available at ScienceDirect

Tetrahedron

journal homepage: www.elsevier.com/locate/tet

Intra- vs inter-molecular electron transfer processes in C–N bond forming reactions. Photochemical, photophysical and theoretical study of 2′-halo-[1,1′-biphenyl]-2-amines

Walter D. Guerra, María E. Budén *, Silvia M. Barolo *, Roberto A. Rossi, Adriana B. Pierini

INFIQC, Departamento de Química Orgánica, Facultad de Ciencias Químicas, Universidad Nacional de Córdoba, Ciudad Universitaria, 5000 Córdoba, Argentina

ARTICLE INFO

Article history:
Received 30 June 2016
Received in revised form 12 August 2016
Accepted 16 August 2016
Available online 25 August 2016

Keywords:
Electron transfer
Photochemical
Arylation reaction
$S_{RN}1$
Radical anions

ABSTRACT

N-Arylation reaction is obtained when 2′-halo-[1,1′-biphenyl]-2-amines are irradiated in basic medium. On the basis of photochemical, photophysical experiments and computational studies we propose that carbazoles are formed by intermolecular electron transfer via $S_{RN}1$ mechanism.
In general, biphenylamines with an EDG like Me or OMe behave in the same way as H giving both, cyclized and reduced products. On the other hand, biphenylamines containing EWG like CN, COOEt or CF_3 gave only the corresponding carbazole. Herein, we report for the first time the chain length for the propagation cycle of intramolecular $S_{RN}1$ reactions and explain that differences in the distribution of products suggest differences regarding the overall mechanism involved.

1. Introduction

Aromatic nucleophilic photosubstitution has proven to be a versatile tool in organic synthesis. The photosubstitution reactions between an aromatic substrate and a nucleophile could be achieved by several mechanisms and its classification is based on the key intermediates involved.[1] When the first step involves the excitation of the substrate in photosubstitution mechanisms, the substrate in its excited state could achieve product, for example, by: heterolysis and S_N1Ar^* via cation phenyl intermediate,[2] S_N2Ar^* (addition–elimination mechanisms)[3] (Scheme 1) or via electron transfer process (ET),[4] among others.

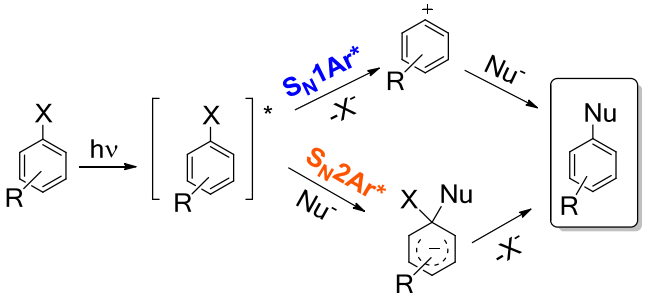

Scheme 1. Polar photosubstitution mechanisms.

We could classify the mechanisms involving ET processes in photo-oxidations (via radical cation intermediates, Scheme 2) or photo-reductions (via radical anion intermediates, Scheme 3). The oxidative ET processes are more common with electron-donating substituted aromatics in water or other ionic solvents (unless a good nucleofugal group is present). The resulting radical cation may react with a nucleophile and the resulting radical ends with rearomatization (Scheme 2).[5] A reductive ET commonly requires the presence of donors such as enolate ions, amines, arenes or alkenes. Mechanisms involving reductive ET processes include $S_N(ET)Ar^*$, radical–radical collapse, $S_{RN}1$ chain process[6] or other photochemical processes. The intramolecular version of reductive ET mechanisms was used for ring closure systems (Scheme 3).

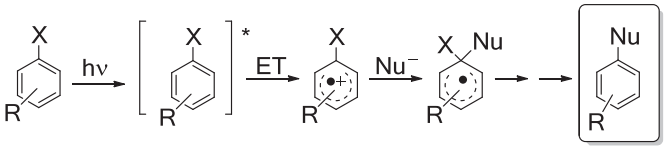

Scheme 2. Oxidative electron transfer mechanism.

* Corresponding authors. E-mail addresses: eugebuden@yahoo.com.ar (M.E. Budén), sbarolo@fcq.unc.edu.ar (S.M. Barolo).

http://dx.doi.org/10.1016/j.tet.2016.08.051
0040-4020/

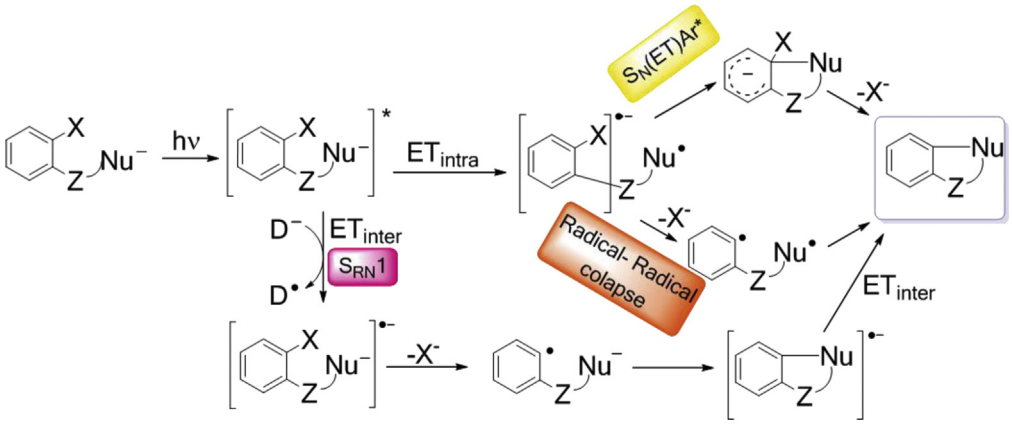

Scheme 3. Aromatic nucleophilic photosubstitution mechanisms by reductive electron transfer.

The reductive ET mechanisms have been proposed for the synthesis of several heterocycles systems. For example, Park *et al.* proposed an intramolecular $S_N(ET)Ar^*$ mechanism (Scheme 3) for the synthesis of 2-pyridinylbenzoxazole from *N*-(2-halophenyl) pyridinecarboxamide[7] and the synthesis of 2-(4-*R*-phenyl)-1,3-benzoxazole and 9-*R*-phenanthridin-6(5*H*)-one from 2′-chloro-4-*R*-benzaniline.[8] The same mechanism was proposed for the synthesis of benzoxazole[3,2-*b*]isoquinolin-11-one from tetrahydroisoquinoline-1,3-diones under basic media.[9] On the other hand, indolo benzoxazoles were prepared from *N*-(2-halophenyl)-indolo-carboxamides,[10] and substituted indazoles from (*Z*)-2-bromoacetophenone *N*-tosylhydrazones with a catalytic amount of *trans-N,N′*-dimethylcyclohexane-1,2-diamine[11] via radical-radical collapse mechanism (Scheme 3).

An $S_{RN}1$ synthetic strategy (Scheme 3) to obtain heterocyclic compounds has been recently applied to the synthesis of 1-phenyl-1-oxazolinoindan derivatives and their related compounds;[12] tetracyclic isoquinoline derivatives;[13] a series of substituted 9*H*-carbazoles[14,15] and carbolines,[16] pyrroles, indoles, and pyrazoles,[17] pyrido[1,2-*a*]benzimidazoles,[18] dibenzosultams from *N*-aryl-2-halobenzenesulfonamides by intramolecular C–C photoinduced arylation,[19] or by visible-light-promoted denitrogenative cyclization of 1,2,3,4-benzothiatriazine-1,1-dioxides,[20] in addition to other heterocyles.[21] However, studies of photochemical and photophysical properties still remain under script in intramolecular $S_{RN}1$ approach.

The varied panorama illustrates that different pathways could be possible and the actual path followed, as well as efficiency of the overall reaction, will depend on a host of factors such lifetime of the singlet or triplet excited state, their redox properties, chemical reactivity and nature of the nucleophile/electron donor, medium and so on. Developing a comprehensive demonstration of the mechanisms involved is not simple and in many cases computational data appear as a supporting and complementary tool.[22]

We recently reported the intramolecular C–N bond forming reactions of 2′-halo-[1,1′-biphenyl]-2-amines to synthesize different 9*H*-carbazoles (Scheme 4).[15] Even the $S_{RN}1$ reaction was proposed to be in play, a full mechanism description is here reported. In general, biphenylamines with an electron donating group (EDG) like Me or OMe behave in the same way as H giving both, cyclized and reduced products. On the other hand, biphenylamines containing electron-withdrawing groups (EWG) like CN, COOEt or CF_3 gave only the corresponding carbazole. These differences in the distribution of products suggest differences regarding the overall mechanism involved.

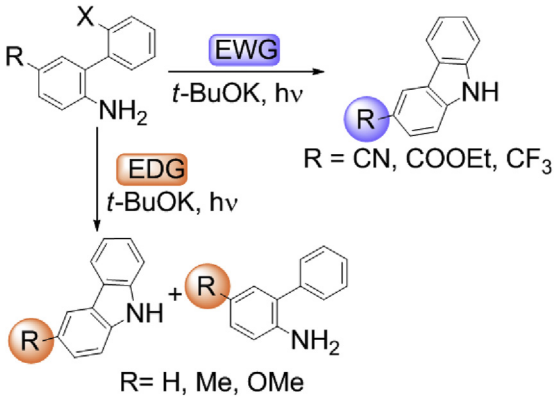

Scheme 4. Intramolecular C–N bond forming reaction and reduction of 2′-halo-[1,1′-biphenyl]-2-amines.

Our proposal is to investigate the mechanism of this photosubstitution from the study of experimental reaction conditions, photophysical properties (UV–vis, steady state fluorescence and time-resolved fluorescence), photochemical studies (the quantum yields measured) and computational data (M06-2X DFT functional and 6-311+G* basis set). Herein, we report for the first time the chain length for the propagation cycle of intramolecular $S_{RN}1$ reactions.

2. Results and discussion

The photostimulated reaction (45 min) of 2′-chloro-[1,1′-biphenyl]-2-amine **1a** in the presence of *t*-BuOK (2 equiv) as a base in DMSO afforded 9*H*-carbazol **2a** in 26% yield and [1,1′-biphenyl]-2-amine **3a** in 17% yield, with a ratio of cyclized versus reduced products of 1.5:1 (Table 1, entry 1). The reaction was completed after 180 min and the ratio between cyclic and reduced product went up to 4.4:1 (57% yield of **2a** and 13% yield of **3a**; entry 2). This reaction is completely suppressed in dark conditions, excluding a benzyne and other polar mechanisms (entry 3). The addition of 25 mol% of *m*-dinitrobenzene (*m*-DNB), a well-known electron acceptor, caused 46% of inhibition (14% yield of **2a**, entry 4). The same behavior was observed when 50 mol% of *m*-DNB was added (85% of inhibition, 4% yield of **2a**, entry 5). The reduced product followed the same tendency. Here, the inhibition was proportional to the amount of *m*-DNB used, showing that ET processes are involved in the formation of products **2a** and **3a** and a chain process could be involved for **2a**.

Table 1
Photostimulated reactions of biphenylamines **1a**–**c** in DMSO[a]

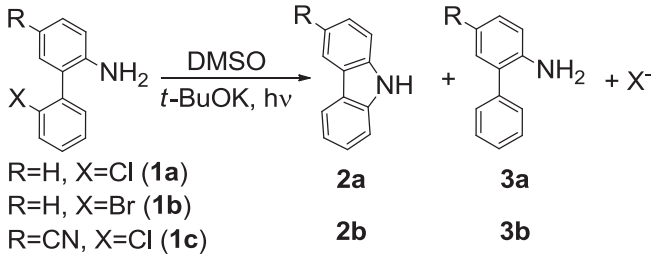

Entry	Biphenylamine **1a**–**c**, yield	Reaction condition	Yield of **2**[b]	Yield of **3**[b]
1	**1a**, 56	45 min, hν	26	17
2	**1a**, —	180 min, hν	57	13
3	**1a**, 84	45 min, dark	—	—
4	**1a**, 70	45 min, hν, 25% mol *m*-DNB	14	6
5	**1a**, 81	45 min, hν, 50% mol *m*-DNB	4	4
6[c]	**1a**, 84	45 min, hν, NaH	—	—
7	**1a**, 23	45 min, hν, O_2	38	—
8	**1b**, 41	45 min, hν	25	21
9	**1a**, 24 and **1b**, 19	45 min, hν	47	16
10	**1c**, 25	15 min, hν	68	—
11	**1c**, 8	45 min, hν	90	—
12[c]	**1c**, 14	45 min, hν, NaH	71	7
13	**1c**, 93	45 min, dark	—	—
14[c]	**1c**, 96	45 min, NaH, dark	—	—
15	**1c**, 58	15 min, hν, 25% mol *m*-DNB	33	—

[a] Photostimulated reactions were performed in inert atmosphere (nitrogen) with [**1a**–**c**]=0.1 M and [*t*-BuOK]=0.2 M in DMSO. Irradiation was conducted in a reactor equipped with two high-pressure lamps of model Phillips HPI-T plus 400 W (air- and water-refrigerated), effective wavelength irradiation longer than 350 nm.
[b] Determined by GC using the internal standard method, error 5%.
[c] 2 equiv of NaH instead *t*-BuOK was used as a base.

It is known that *t*-BuO^- anion is a good electron donor.[23] With the aim of determining whether the reaction was initiated by ET from *t*-BuO^- anions to the substrate, the reaction was carried out without *t*-BuO^- anions, but in the presence of NaH as a base. Under this condition, no products were found (entry 6).

To elucidate the reaction mechanisms, the photo-substitution reaction was carried out in the presence of oxygen atmosphere (entry 7). In this case, product **2a** was obtained in 38% yield while reduction product **3a** was completely inhibited. These results imply that the single excited state of biphenylamine **1a** may be mainly involved in the photo-substitution product **2a** and triplet state may be involved in the reduced product **3a**.[7]

The photostimulated reaction proceeded with the precursor (2′-bromo-[1,1′-biphenyl]-2-amine, **1b**) under the same conditions to yield cyclized and reduced products **2a**–**3a** (25% yield of **2a** and 21% yield of **3a**; entry 8) with a ratio close to 1.2:1. The competition experiment between bromo and chloro derivatives, **1a** and **1b**, was calculated according to Eq. 1 [24] (entry 9). We found that the bromo precursor is 1.3 times more reactive than chloro precursor, in agreement with the reactivity order of an ET reaction.

$$\text{global}\ \frac{k_{Br}}{k_{Cl}} = \frac{k_{\mathbf{1b}}}{k_{\mathbf{1a}}} = \frac{\ln([\mathbf{1a}]_0/[\mathbf{1a}]_0 - [\mathbf{1a}]_t)}{\ln([\mathbf{1b}]_0/[\mathbf{1b}]_0 - [\mathbf{1b}]_t)} \quad (1)$$

When 2′-chloro-5-carbonitrile-[1,1′-biphenyl]-2-amine (**1c**) was used as a substrate model for EWG, only cyclic product **2b** was obtained in 68% and 90% yield, after 15 and 45 min of irradiation, respectively (entries 10 and 11). Unlike chlorinated substrate **1a**, photostimulated reaction of biphenyl amine **1c** in the presence of NaH as a base (instead *t*-BuO^- anions) gave cyclic product **2b** in 71% yield together with 7% yield of **3b** (entry 12). Both reactions (with *t*-BuOK and NaH as bases) were inhibited in dark conditions (entries 13 and 14). Moreover, the addition of 25% mol of *m*-DNB caused 51% of inhibition (33% yield of **2b**, entry 15). These results indicate that anion **1c**$^-$ rather than *t*-BuO^- anion acts as a donor in the initial ET (homo-coupled redox reaction) and this step is induced by light.

To support our initial evidence of the mechanism, we performed different studies with steady-state and time-resolved fluorescence. First, we studied photophysical properties of the anions involved (anions **1a**$^-$, **1b**$^-$, **1c**$^-$ and **3a**$^-$). UV–vis absorption spectra of the anions were measured in DMSO under nitrogen atmosphere.[25] It is important to notice that both neutral and anion absorbed in the same region for pairs **1a**/**1a**$^-$ (Fig. 1A), **1b**/**1b**$^-$ and **3a**/**3a**$^-$, with almost identical λ_{max}, but substantially changed for **1c**/**1c**$^-$ (Fig. 1B).

Since the shape of the UV spectra of neutral and anion is almost identical, we could not determine the proportion of base required to complete the formation of the corresponding anion. To solve this problem, we performed a steady-state fluorescence titration with increasing amounts of base (*t*-BuOK). The preparation of anion **1a**$^-$ is shown as an example in Figure 1C. During titration, the band corresponding to the neutral species disappeared (λ_{em}=340–380 nm) and a new band at a longer wavelength was observed (λ_{em}=410–470 nm), attributed to anion **1a**$^-$. With this procedure, we determined that 10 equiv of *t*-BuOK were necessary to completely form anion **1a**$^-$, 20 equiv for **1c**$^-$ and 50 equiv for **3a**$^-$.[25]

Furthermore, for all the anions, emission and excitation steady-state fluorescence spectra were acquired[25] and excited singlet state energy (E_{0-0}) was estimated (Table 2). Relative fluorescence quantum yields (Φ_f) for all anions were also calculated using anthracene as a reference[26] (Table 2). The relative fluorescence quantum yield for dehalogenated anion **3a**$^-$ was greater than those for halogenated anions (**1c**$^-$>**1a**$^-$>**1b**$^-$). For anion **1c**$^-$ Φ_f was bigger than that of the other halogenated anions which could be related to more efficient fluorescence decay from excited singlet state.

The photoinduced reductive ET could be an intramolecular or intermolecular process (bimolecular) where the substrate in excited state receives an electron from a corresponding donor (Scheme 3). If ET_{inter} is taking place, the donor could be the substrate (corresponding anion) or the base (*t*-BuO^- anion). To reveal which donor is involved we performed a steady-state and time-resolved fluorescence quenching study.

All anions experimented steady-state fluorescence quenching with *t*-BuO^- anion and followed Stern–Volmer linear relationship (Eq. 2),[27]

$$\frac{I_0}{I} = 1 + K_{SV}\left[t\text{–}BuO^-\right] \quad (2)$$

where I_0 and I are fluorescence intensities (or areas) in the absence or presence of the quencher respectively, [*t*-BuO^- anion] is the concentration of quencher, and K_{sv} is the Stern–Volmer quenching constant. As shown in Figure 2A, increasing concentrations of *t*-BuO^- anion decreases the fluorescence intensity (or total area) of anion **1a**$^-$, while shape and maxima of the emission spectra remained unchanged. This indicates that no exciplex formation is implicated in the quenching mechanisms. Table 3 shows the static K_{SV} quenching constant values.

As observed in Figure 2B, anion **1c**$^-$ seemed not to have quenching process; however, at a higher concentration of *t*-BuO^- anion (more than 2500 equiv of *t*-BuO^- anion) subject had a quenching with a K_{SV} of $(3.4\pm0.1)\times10^2$ M^{-1} (Table 3).

Next, we evaluated the effect of *t*-BuO^- anion added to the singlet state lifetime (τ_f) of anions **1a**$^-$ and **1c**$^-$ using time-resolved fluorescence measurements. For anion **1a**$^-$ we observed that τ_f changed by addition of *t*-BuO^- anion (dynamic quenching),

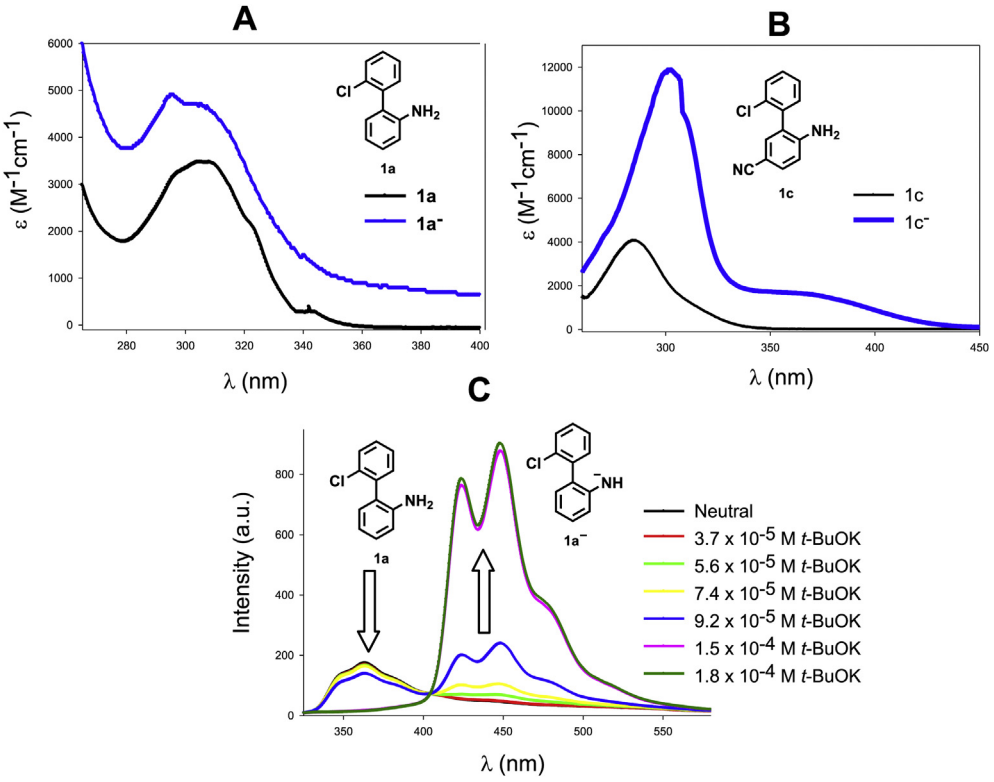

Fig. 1. A) UV–vis spectra for compound **1a** (black solid line, [**1a**]=9.3×10^{-5} M) and anion **1a**$^-$ (blue solid line, [**1a**$^-$]=2×10^{-5} M). B) UV–vis spectra for compound **1c** (black solid line, [**1c**]=8.3×10^{-5} M) and anion **1c**$^-$ (blue solid line, [**1c**$^-$]=4.1×10^{-6} M) in DMSO under N_2 atmosphere. C) Steady-state fluorescence titration with *t*-BuOK for biphenyl amine **1a** ([**1a**]=2×10^{-5} M) in DMSO under N_2 atmosphere. Fluorescence emission spectra were collected using an excitation wavelength of 305 nm.

Table 2
Photophysical properties for neutral (**1a**–**c** and **3a**) and anions (**1a**–**c**$^-$ and **3a**$^-$) in DMSO[a]

Comp.	λ_{max} abs neutral[b]	λ_{max} abs anion[b]	λ_{max} exc[b] anion	λ_{max} em[b] anion	E_{0-0}[c]	Φ_f anion[d]
1a	305	305	297, 334	348, 364	84.6	0.03
1b	312	306	297, 320, 397, 417	423, 449, 477	72.6	0.02
1c	284	302, 348	305, 355	398, 440	77.9	0.37
3a	313	313	276, 322	408	78.8	0.96

[a] All UV–vis and fluorescence spectra were recorded in N_2 atmosphere and DMSO as a solvent.
[b] Wavelength (λ) is given in nm.
[c] Values for E_{0-0} are given in kcal mol^{-1} and were determined from the intersecting wavelength of the normalized excitation and emission spectra of the anions.
[d] Fluorescence quantum yields (Φ_f) for anions were estimated using anthracene in EtOH (Φ_f=0.27) as a Ref. 26.

Table 3
Quenching values for anions **1a**$^-$, **1b**$^-$, **1c**$^-$ and **3a**$^-$

Comp.	Relation [anion]/[*t*-BuO$^-$]	Static K_{SV}—*t*-BuO$^-$ (10^2 M^{-1})[a]	Dynamic K_{SV}—*t*-BuO$^-$ (M^{-1})[b]	Dynamic K_{SV}-anion (M^{-1})[c]
1a$^-$	9–61	(8.9±0.3)	(8.0±0.8)×10^2	No quenching
1b$^-$	40–112	(8.5±0.7)	—	—
1c$^-$	2500–4500	(3.4±0.1)	No quenching	(1.2±0.2) x10^6
3a$^-$	3–210	(1.73±0.03)	—	—

[a] Values obtained from linear regression of I_0/I as a function of [*t*-BuO$^-$ anion].
[b] Values obtained from τ_0/τ as a function of [*t*-BuO$^-$ anion].
[c] Values obtained from τ_0/τ as a function of [**1a**$^-$] or [**1c**$^-$].

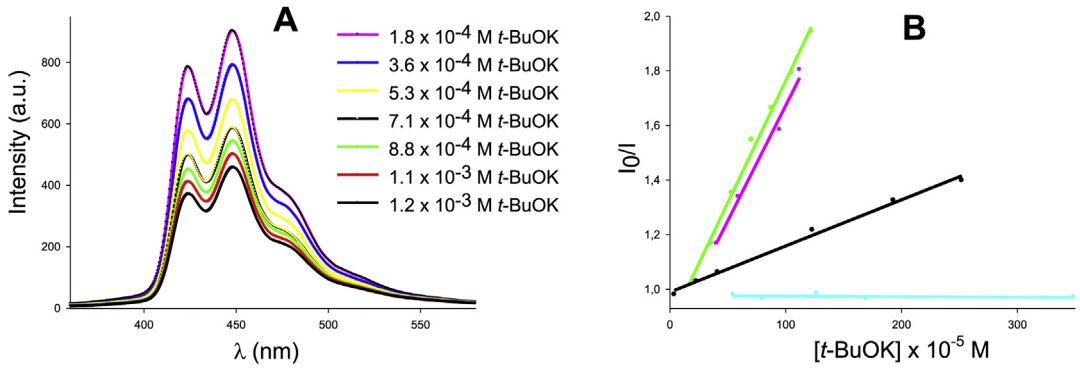

Fig. 2. A) Fluorescence emission spectra of anion **1a**$^-$ with *t*-BuO$^-$ anion as a quencher. The concentration of **1a**$^-$ was fixed at 2×10^{-5} M; [*t*-BuO$^-$ anion] from 18 to 122×10^{-5} M; T=298 K, λ_{exc}=305 nm. Both excitation and emission slits were 10 nm. B) Stern–Volmer plots for **1a**$^-$ (—), **1b**$^-$ (—), **1c**$^-$ (—) and **3a**$^-$ (—).

indicating that the excited state of the biphenylamine anion **1a**$^-$ interacts with *t*-BuO$^-$ anion (ET process). However, for this anion, fluorescence lifetime remained constant by increasing anion concentration (Fig. 3). In contrast, for anion **1c**$^-$, τ_f remained unchanged at different concentrations of *t*-BuO$^-$ anion (in the range that steady-state fluorescence quenching was performed, Fig. 3A). Increasing the anion concentration of **1c**$^-$, we observed changes in τ_f, indicating the presence of self-quenching in the single excited state (Fig. 3B). All these results have allowed us to conclude that we are in the presence of a mechanism initiated by an ET_{inter} ($S_{RN}1$ mechanisms), dynamic K_{SV} showing a 10^4 magnitude order higher for **1c**$^-$ than for **1a**$^-$ (Table 3).

$$\Delta G_{ET}^{*} = \frac{\lambda}{4}\left(1+\frac{\Delta G_{rel}}{\lambda}\right)^2 \quad (3)$$

where ΔG_{rel} represents the relative free energy difference between the reactive and products, and λ is the reorganization energy (interpreted as the vertical energy difference between the minimum of the product curve and the point where the reactant curve overlaps with this on the potential energy surface).

Scheme 5 summarizes the different activation free energy ΔG_{ET}^{*}. In both cases, we can find that the process is more endergonic from the ground state than from the excited state. Further, for anion **1a**$^-$,

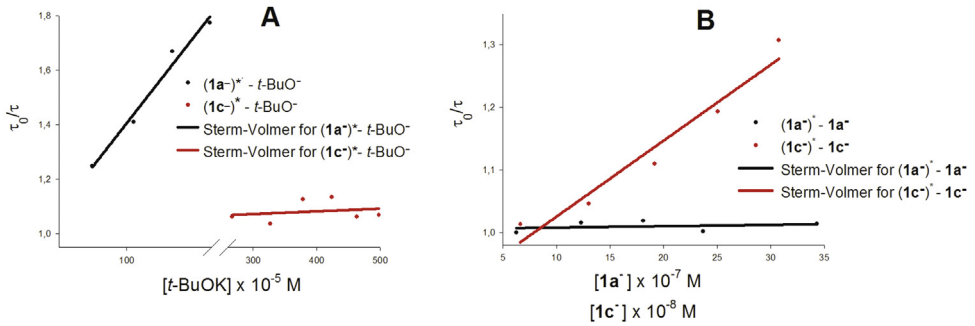

Fig. 3. A) Stern–Volmer plots for **1a**$^-$ or **1c**$^-$—*t*-BuO$^-$ anion system. B) Stern–Volmer plots for **1a**$^-$ and **1c**$^-$ with the corresponding anion as a quencher (self-quenching).

In order to support the photophysical and photochemical phenomena observed in anions **1a**$^-$ and **1c**$^-$ and to understand the nature of the ET involved in the initiation step, we carried out computational calculations. Our study was performed from the excited state of anions **1a**$^-$ and **1c**$^-$ using M06-2X as functional,[28] 6-311+G* basis set in polarized continuum model (PCM).[29] The study in excited state was carried out employing TD-DFT with the same functional and basis set.

Figure 4 shows the ground and singlet excited states of both **1a**$^-$ and **1c**$^-$. It is important to notice that both anions in the excited state (after optimization) exhibit distortions in both dihedrals, the one that involved C–Cl experimenting a bending, and the biphenyl moiety dihedral. This change in structure could be related to the changes in photo-physical properties between the ground and the excited state.

In addition to study the initiation step, we employed the Marcus–Hush theory[30] to calculate the activation free energy (ΔG_{ET}^{*}) involved in an outer-sphere ET (Eq. 3)

ET reaction from *t*-BuO$^-$ anion to excited state of (**1a**$^-$)* is favored than homo-coupled redox reaction (11.52 vs 17.20 kcal mol^{-1}, respectively). By contrast, for anion **1c**$^-$, we found that ΔG_{ET}^{*} is slightly favored from the excited anion (**1c**$^-$)* rather than from *t*-BuO$^-$ anion (11.80 vs 12.06 kcal mol^{-1}). These results are consistent with those found in experimental quenching (Fig. 3).

In addition, we evaluated the feasibility of different steps (fragmentation, C–N coupling and ET_{inter}[31] for propagation step and hydrogen abstraction) of the proposed mechanism by DFT calculations, and anions **1a**$^-$ and **1c**$^-$ were taken as representatives. The main results for activation energies for all the steps mentioned are summarized in Figure 5. The evaluation of these activation energies leads us to conclude that there is not major difference in Ea_{C-N}, Ea_{ET} or $Ea_{abstraction}$ that may account for the presence of reduced product (**3a**) in the cyclization reaction of **1a**$^-$. The only difference found was that $Ea_{fragmentation}$ for **1c**$^-$ is twice bigger than that for **1a**$^-$. Moreover, **1a**$^-$ cyclizes with lower activation energy than **1c**$^-$ (6.0 kcal mol^{-1} vs

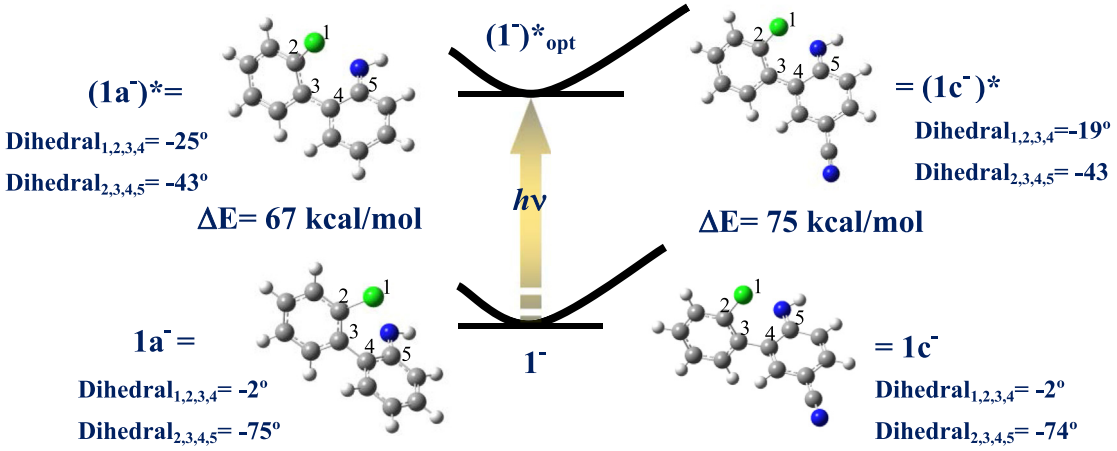

Fig. 4. Representation of anions **1a**$^-$ and **1c**$^-$ in ground and singlet excited states.

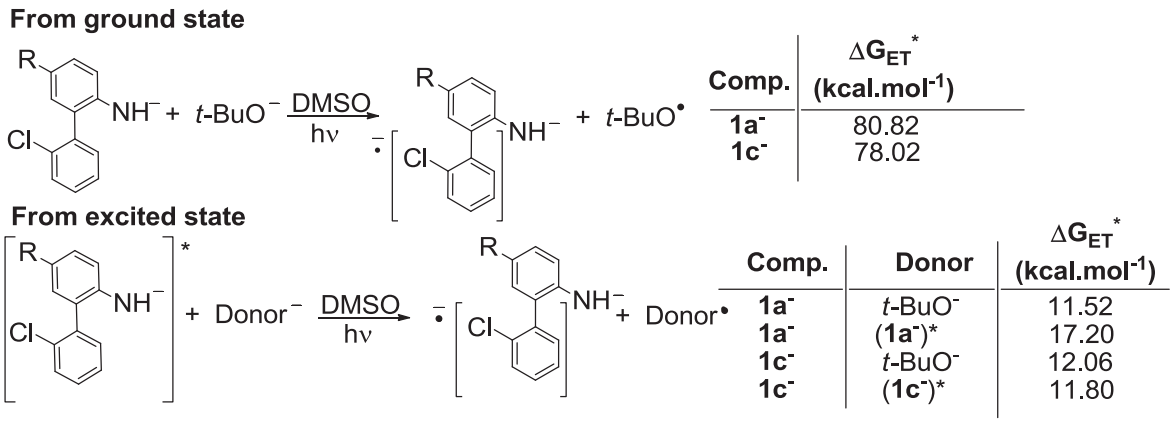

Scheme 5. Calculations of activation free energy (ΔG_{ET}^{*}) for ET reactions from ground and excited state by Marcus–Hush theory.

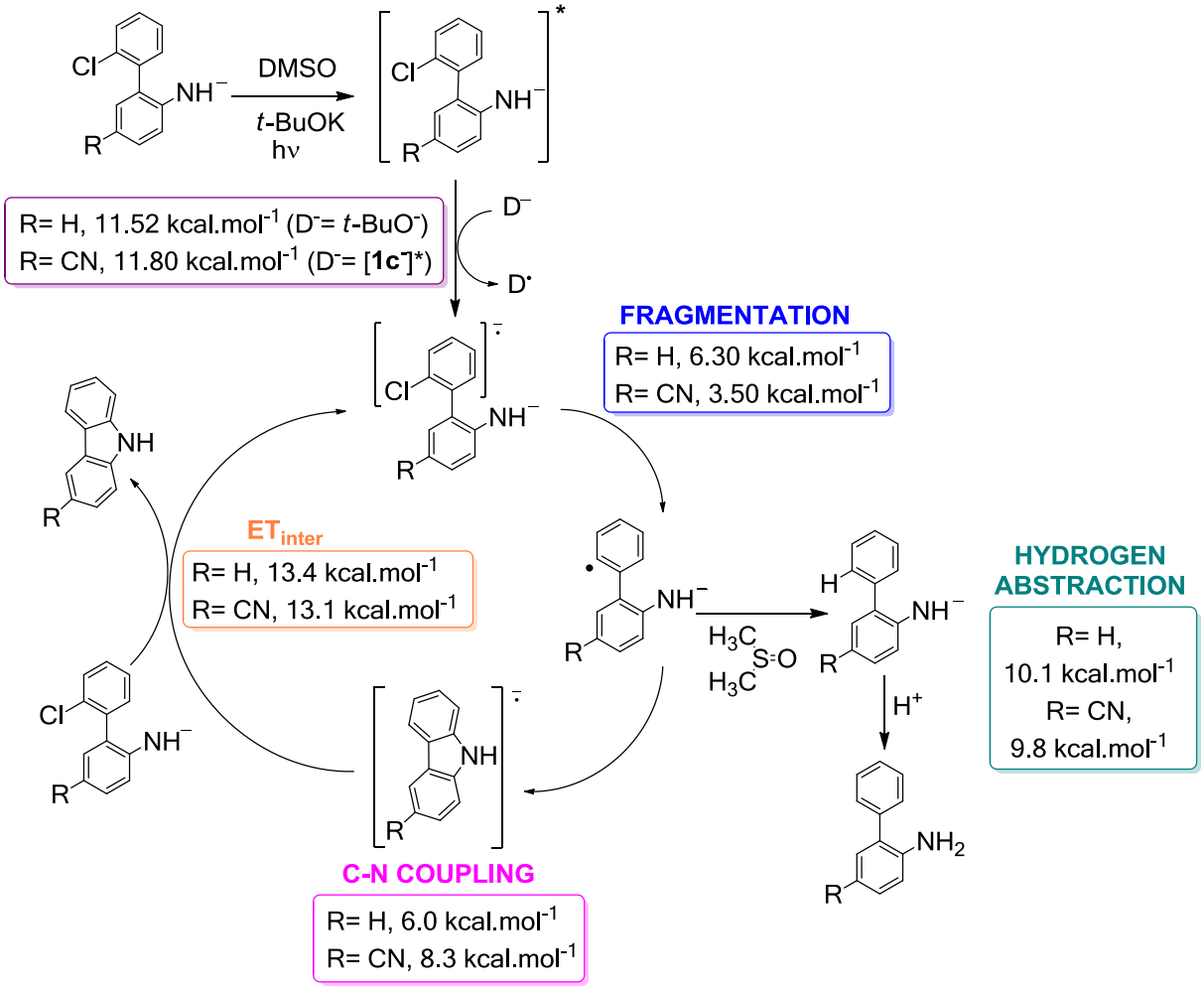

Fig. 5. Activation energies for different steps in the mechanisms proposed.

8.3 kcal mol^{-1}). We also analyzed the hydrogen-abstraction reaction by inclusion of a discrete molecule of the solvent (DMSO), and found that this step is higher in energy to compete with C–N coupling.[32]

The $S_{RN}1$ reaction is a chain mechanism, hence the overall reactivity, as well as the quantum yield of the products (Φ_{global}), depends on the efficiency of the initiation, propagation and termination steps. The magnitude of the chain length ($\Phi_{propagation}$) could be calculated by the ratio of the overall quantum yield and the quantum yield of the initiation step ($\Phi_{initiation}$) (Eq. 4).[33]

$$\text{Chain}\cdot\text{Length} = \Phi_{propagation} = \frac{\Phi_{global}}{\Phi_{initiation}} \quad (4)$$

To calculate the quantum yield of the initiation step ($\Phi_{initiation}$) we proposed two different approximations. The first one includes the suppression of the substitution product (cyclized product) by

the addition of a good hydrogen donor like 1,4-cyclohexadiene. In this condition the main product formed is reduced product (Eq. 5). The second approximation involves the use of biphenylamine **1d**. This precursor could only afford the reduced product **3a** (Eq. 6).

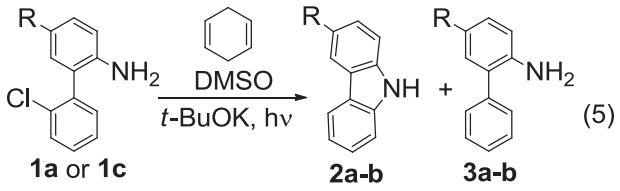

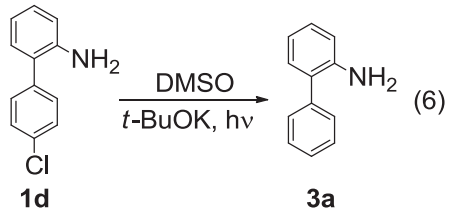

Our measurements of quantum yields were performed at λ=300 nm.[34] For **1a**, $\Phi_{initiation}$ was calculated from both approximations reaching a similar chain length around 2 (Table 4, entries 1–3). This was achieved since the addition of 1,4-cyclohexadiene was a good way to suppress the product cyclized. For **1c** chain length was calculated; it was more than twice than for **1a** ($\Phi_{propagation}$=4.8) (Table 4, entry 6). In this case, the propagation step could not be calculated suppressing the cyclized product (Eq. 5) due to the fact that the cyclization process was more efficient for **1c** than for **1a**. The difference in $\Phi_{propagation}$ could be related to the fact that the turnover of the reaction for **1c** was larger than for **1a**. These results could account for the difference in the distribution product found.

Table 4
Quantum yields and chain length calculated for anions **1a**$^-$ and **1c**$^-$[a]

Entry	Biphenylamine—**1**[b]	Φ products[c]		Chain length
		2	**3**	
1	**1a**	**2a**, 5.4	**3a**, 6.1	1.8
2[d]	**1a**	**2a**, 0.1	**3a**, 9.4	
3[e]	**1d**	—	**3a**, 5.4	2.1
4	**1c**	**2b**, 7.3	**3b**, 1.8	n.d.
5[d]	**1c**	**2b**, 12.2	**3b**, 3.5	
6[f]	**1d**	—	**3b**, 1.9	4.8

[a] Performed under N_2 atmosphere, using [**1a**] or [**1c**]=0.1 M and [*t*-BuOK]=0.2 M in DMSO. Irradiation was conducted in a photoreactor (Rayonet) equipped with 10 lamps of Hg (air refrigerated), effective wavelength irradiation at 300 nm. The products were quantified by GC using the internal standard method.
[b] For **1a** the reaction time was 45 min; for **1c** the reaction time was 12 min.
[c] Determined at λ_{max}=300 nm using Fe(III) as actinometer.
[d] In the presence of 0.5 M of 1,4-cyclohexadiene.
[e] Irradiated for 45 min for comparison with **1a**.
[f] Irradiated for 12 min for comparison with **1c**.

3. Conclusions

Here, a complete mechanistic picture of the photoinduced ET cyclization reaction is discussed. A comparative and detailed study at the initiation level has allowed us to conclude that ET process involves bimolecular interaction ($S_{RN}1$), excluding ET_{intra} mechanisms like S_N(ET)Ar* and radical–radical collapse.

The difference of photophysical properties and photochemical reactivity is in agreement with the nature of the initiation step. For anion **1a**$^-$ is proposed that ET from *t*-BuO$^-$ anion to (**1a**$^-$)* could be involved meanwhile for **1c**$^-$ homo-coupled redox reaction take place. The computational data using Markus–Hush from the excited state show a similar tendency than that of the photophysical study.

Our study involves the first calculation of a chain length in an intramolecular $S_{RN}1$ process finding that **1c** has twice chain length than **1a**. Both initiation and propagation could be involved in favor to the formation of only one product for **1c** (cyclized product **3c**), under $S_{RN}1$ mechanism.

4. Experimental section

4.1. Computational procedure

All calculations were performed with the Gaussian09 program. The conformers obtained were refined with complete geometry optimization within the M06-2X DFT functional and 6-311+G* basis set. The geometries thus found were used as starting points for the evaluation of the reaction profiles by using the distinguished reaction coordinate scan. The effect of DMSO as a solvent was evaluated through Tomasi's Polarized Continuum Model (PCM) as implemented in Gaussian09. The inclusion of the solvent in the calculations is a requisite for evaluating valence radical anions. The characterization of stationary points was done by Hessian matrix calculations. The energy informed for TSs, anions and radical anions includes zero-point corrections. The vertical excited singlet stated (^{1}S) of anion **3a** was calculated with TD-DTF, the M06-2X functional and the 6-311+G* basis set. The energy of ^{1}S was calculated including PCM contribution under the state-specific approach. After vertical excitation the singlet excited state was optimized with the same functional and basis set.

4.2. General considerations

Column chromatography was carried out on silica gel. Melting points were determined using a standard melting point instrument and were uncorrected. Gas chromatographic analyses were performed with a flame-ionization detector, on 30 m capillary column of a 0.32 mm×0.25 μm film thickness, with a 5% phenylpolysiloxane phase. GC–MS analyses were performed employing a 25 m×0.2 mm×0.33 μm with a 5% phenylpolysiloxane phase column. ^{1}H NMR spectra and ^{13}C NMR spectra were recorded on a 400.16 MHz in $CDCl_3$ or Dimethyl sulfoxide-d_6 (CD_3SOCD_3) as solvent with TMS as internal standard. Coupling constants are given in Hz and chemical shifts are reported in δ values in ppm. Data are reported as follows: chemical shift, multiplicity (s=singlet, br s=broad singlet, d=doublet, t=triplet, dd=double doublet, dt=double triplet, ddd=double double doublet, m=multiplet), coupling constants (Hz), and integration. Copies of ^{1}H NMR and ^{13}C NMR spectra are provided in SI.

4.3. General methods and materials

4.3.1. Methods. Irradiation was performed in a photochemical reactor equipped with two HPI-T 400 W lamps metallic iodide (air and water refrigerated). Irradiation for quantum yield was carried out using 10 lamps of 300 nm each in a photochemical reactor (Rayonet) at room temperature (air refrigerated). The purification of the products was done by column chromatography on silica gel. Gas chromatographic analyses were obtained with a flame-ionization detector, on 30 m capillary column of a 0.32 mm×0.25 μm film thickness, with a 5% phenylpolysiloxane phase. Quantification by GC was performed by the internal standard method. Mass spectra were performed employing a 25 m×0.2 mm×0.33 μm with a 5% phenylpolysiloxane phase column. ^{1}H NMR (400.16 MHz) and ^{13}C NMR (100 MHz) spectra were obtained in $CDCl_3$ or DMSO-d_6 as solvents. Coupling constants (J) are given in Hz units and chemical shifts are reported in δ values in ppm. Melting points were recovered with an Electrothermal 9100 instrument and were uncorrected.

4.3.2. Materials. *9H-carbazol*, [1,1′-biphenyl]-2-amine, *t*-BuOK, NaH, *m*-DNB, TEMPO, 1,4-cyclohexadiene, anthracene were commercially

available and used as received from the supplier. DMSO was stored under molecular sieves (4 Å). All solvents were analytical grade. Silica gel (0.063–0.200 mm) was used in column chromatography.

4.3.3. Spectroscopic measurements. The UV–vis and the spectrofluorimetric determinations were carried out in a Shimadzu UV-2101 PC and a Jasco FP-777, respectively. All measurements were carried out under an inert atmosphere of nitrogen, in quartz cuvettes, at room temperature. Solutions of *t*-BuOK were prepared at time of use. UV–vis spectra were recorded on UV–vis spectrophotometer. Fluorescence spectra were performed in a fluorescence spectrometer. Fluorescence lifetimes were measured by the single-photon counting technique irradiating with a laser at 340 nm. Quantum yield of fluorescence was determined from the integrated emission spectra, using anthracene as the reference following the methods reported.

4.3.4. Total quantum measurements.[35] The ferrioxalate actinometer was prepared by mixing equal volumes of 0.02 M ammonium ferric sulfate dodecahydrate with 0.06 M potassium oxalate-1-hydrate both in 0.1 N H_2SO_4 in the dark. After illumination the product Fe(II) was analyzed by adding 0.5 mL of 0.1% (w/v) 1,10-phenanthroline monohydrate in 1.8 M anhydrous sodium acetate to 3 mL of the actinometer. The absorbance of $[Fe(1,10\text{-phen})_3]^{2+}$ was measured after 30 min in the dark $\varepsilon_{510}=(5.9\pm0.3)\times 10^3\ M^{-1}\ cm^{-1}$ for the calculation of concentration.

4.4. Representative procedure for synthesis of 2′-halo-[1,1′-biphenyl]-2-amines

The procedure for the synthesis of biphenylamines **1a**–**c** followed previous reports.[15]

*4.4.1. 2′-Bromo-[1,1′-biphenyl]-2-amine (**1b**).*[36] The product was purified by column chromatography on silica gel eluting with petroleum ether/EtOAc (100:0→95:5%). Brown solid was obtained in 70% yield (0.17 mg, 0.7 mmol). ^{1}H NMR (400 MHz, $CDCl_3$): δ 7.69 (dd, *J*=8.0, 0.8, 1H), 7.38 (td, *J*=7.4, 1.2, 1H), 7.32 (dd, *J*=7.6, 2.0, 1H), 7.18–7.25 (2H, m), 7.02 (dd, *J*=7.4, 1.2, 1H), 6.82 (td, *J*=7.4, 1.2, 1H), 6.77 (dd, *J*=8.0, 0.8, 1H), 3.52 (br s, 2H); ^{13}C NMR (100 MHz, $CDCl_3$): δ 143.5, 140.0, 133.1, 131.8, 130.2, 129.2, 129.1, 127.8, 127.1, 124.2, 118.2, 115.5. GC–MS (EI) *m*/*z* 249 (M^++2, 12), 247 (M^+, 8), 169 (14), 168 (100), 167 (79), 140 (12), 139 (16), 84 (25), 83 (10).

*4.4.2. 4′-Chloro-[1,1′-biphenyl]-2-amine (**1d**).*[37] A solution of 1-chloro-4-iodobenzene (86 mg, 0.5 mmol), (2-aminophenyl)boronic acid hydrochloride (173.0 mg, 1.0 mmol), $Pd(PPh_3)_2Cl_2$ (70.2 mg, 0.1 mmol), PPh_3 (52.5 mg, 0.2 mmol) and K_2CO_3 (552 mg, 4 mmol) in toluene:ethanol (10:4 mL) was stirred at room temperature for 5 min. H_2O (2 mL) was added, and the resulting mixture was slightly degassed, sealed and stirred at 120 °C for 2 h. After being cooled to room temperature, the mixture was extracted with Et_2O or EtOAc. The extracts were combined, dried over Na_2SO_4, and filtered. After removal of volatile components from the filtrate, the resulting crude product was purified by column chromatography on silica gel eluting with pentane/EtOAc (100:0→80:20%). Light yellow oil was obtained in 75% yield (153 mg, 0.75 mmol). ^{1}H NMR (400.16 MHz, $CDCl_3$): δ 7.40–7.35 (m, 4H), 7.14 (t, *J*=7.6, 1H), 7.06 (d, *J*=7.6, 1H), 6.80 (t, *J*=7.6, 1H), 6.73 (d, *J*=8.0, 1H), 3.68 (br s, 2H); ^{13}C NMR (100.62 MHz, $CDCl_3$): δ 143.3, 137.8, 132.9, 130.3(x2), 130.2, 128.8(x2), 128.7, 126.1, 118.6, 115.6.

4.5. Representative procedure for photostimulated reactions. Preparation of carbazole derivatives in DMSO

The following procedure is representative of all these reactions. They were carried out in a flame-dried Schlenk tube equipped with a nitrogen inlet and magnetic stirrer at rt. To 5 mL of dry and degassed DMSO under nitrogen was added 0.4 mmol (2.0 equiv, 0.449 g) of *t*-BuOK and after 5 min, 0.2 mmol (1 equiv) of biphenylamine. The reaction mixture was irradiated for the corresponding time. If the biphenylamine was oil, it was added dissolved in dry ethyl ether. The reaction was quenched with an excess of ammonium nitrate and water. The mixture was extracted three times with ethyl acetate (30 mL each), the organic extract was washed twice with water, dried over Na_2SO_4 and quantified by GC using the internal standard method.

The procedure for the isolation of carbazoles **2a** and **2b** and reduced product **3a** followed previous reports.[15] Spectroscopy data agreed with the literature.

*4.5.1. 6-Amino-[1,1′-biphenyl]-3-carbonitrile (**3b**).*[39] The procedure for the synthesis of **3b** was followed as Ref. 39. The product was purified by column chromatography on silica gel eluting with pentane/EtOAc (100:0→75:25%). Light yellow crystals were obtained in 88% yield (171 mg, 0.881 mmol). ^{1}H NMR (400.16 MHz, CD_3SOCD_3): δ 7.49–7.37 (m, 6H), 7.33 (d, *J*=2, 1H), 6.82 (d, *J*=8.4, 1H), 5.81 (br s, 2H); ^{13}C NMR (100.62 MHz, CD_3SOCD_3): δ 150.1, 137.9, 134.4, 132.8, 129.4, 129.1, 128.0, 126.0, 120.8, 115.4, 97.3; GC–MS (EI) *m*/*z* 195 (13), 194 (M^+, 98), 193 (100), 192 (37), 166 (11), 83 (12).

4.5.2. 2-Amino-2′-deuteriobiphenyl.[32,38] The reaction was carried out with the same procedure using 2.5 mL of DMSO-d_6. The crude was extracted in acid media (pH=1, H_2SO_4) with ethyl acetate (3×30 mL); the combined organic layers were discarded. The resulting aqueous phase was extracted in basic media (pH=10, NaOH) with ethyl acetate (3×30 mL); washed with H_2O (20 mL) and dried over anhydrous Na_2SO_4; and the solvent was evaporated under vacuum. The product was purified by preparative TLC eluting with pentane/ethyl acetate (98:2%) as a colorless liquid. Spectroscopy data agreed with the literature.

Acknowledgements

We thank Dr. Prof. Guillermo Montich, Universidad Nacional de Córdoba for time-resolved fluorescence facilities. This work was supported in part by Consejo Nacional de Investigaciones Científicas y Técnicas (CONICET) grant number: PIP-2012, Secretaría de Ciencia y Tecnología, Universidad Nacional de Córdoba (SECyT) and Agencia Nacional de Promoción Científica y Técnica (ANPCyT) grant number: PICT 2012-2303. W.D.G. gratefully acknowledges the receipt of a fellowship from CONICET.

Supplementary data

Supplementary data (Copies of UV–vis spectra, steady-state fluorescence spectra, excitation and emission spectra, ^{1}H NMR and ^{13}C NMR spectra for the substrates and products and theoretical section (xyz of stationary points)) associated with this article can be found in the online version, at http://dx.doi.org/10.1016/j.tet.2016.08.051.

References and notes

1. Fagnoni, M.; Albini, A. In *Photonucleophilic Substitution Reactions in Organic Photochemistry and Photophysic*; Ramamurthy, V., Schanze, K., Eds.; CRC Taylor & Francis: Boca Raton, 2006; pp 131–170.
2. (a) Havinga, E.; Cornelisse, J. *Chem. Rev.* **1975**, *75*, 353–388; (b) Yang, N. C.; Huang, A.; Yang, D. H. *J. Am. Chem. Soc.* **1989**, *111*, 8060–8061.
3. Cornelisse, J. Photochemical reactions of arenes with amines In *CRC Handbook of Organic Photochemistry and Photobiology*; Horspool, W. H., Song, P.-S., Eds.; CRC: New York, 1995; pp 250–283.

4. Ceroni, P.; Balzani, V. Photoinduced Energy and Electron Transfer Processes In *The Exploration of Supramolecular System and Nanostructures by Photochemical Techniques*; Ceroni, P., Ed.; Springer Science+Business Media B: 2012, Chapter 2.
5. Fukuzumi, S.; Ohkubo, K. Photoinduced Reactions of Radicals Ions via Charge Separation In *Encyclopedia of Radicals in Chemistry, Biology & Materials*; Chatgilialoglu, C., Studer, A., Eds.; John Wiley & Sons: Chichester, UK, 2012; pp 365–393.
6. For reviews see: (a) Budén, M. E.; Martín, S. E.; Rossi, R. A. Recent Advances in the Photoinduced Radical Nucleophilic Substitution Reactions In *CRC Handbook of Organic Photochemistry and Photobiology*, 3th ed.; Griesbeck, A. G., Oelgemöller, M., Ghetti, F., Eds., 3th ed.; CRC: Boca Raton, 2012; Chapter 15, pp 347–368; (b) Bardagí, J. I.; Vaillard, V. A.; Rossi, R. A. In *The $S_{RN}1$ Reaction in Encyclopedia of Radicals in Chemistry, Biology & Materials*; Chatgilialoglu, C., Studer, A., Eds.; John Wiley & Sons: Chichester, UK, 2012; pp 333–364; (c) Rossi, R. A.; Pierini, A. B.; Peñéñory, A. B. *Chem. Rev.* **2003**, *103*, 71–167; (d) Rossi, R. A.; Guastavino, J. F.; Budén, M. E. In *The $S_{RN}1$ Reaction in "Arene Chemistry: Reaction Mechanisms and Methods for Aromatic Compounds". Part 2. Nucleophilic Aromatic Substitution*; Mortier, J., Ed.; John Wiley & Sons: Chichester, UK, 2016; Chapter 10, pp 243–268.
7. Park, Y.-T.; Jung, C.-H.; Kim, K.-W. *J. Org. Chem.* **1999**, *64*, 8546–8556.
8. Mayouf, A. M.; Park, Y.-T. *J. Photochem. Photobiol., A* **2002**, *150*, 115–123.
9. Senthilvelan, A.; Ramakrishman, V. T. *Tetrahedron Lett.* **2002**, *43*, 8379–8381.
10. Vaillard, V. A.; Rossi, R. A.; Argüello, J. E. *Org. Biomol. Chem.* **2012**, *10*, 9255–9261.
11. Thomé, I.; Besson, C.; Kleine, T.; Bolm, C. *Angew. Chem., Int. Ed.* **2013**, *52*, 7509–7515.
12. Marshall, L. J.; Roydhouse, M. D.; Slawin, A. M. Z.; Walton, J. C. *J. Org. Chem.* **2007**, *72*, 898–911.
13. Roydhouse, M. D.; Walton, J. C. *Eur. J. Org. Chem.* **2007**, 1059–1063.
14. Budén, M. E.; Vaillard, V. A.; Martín, S. E.; Rossi, R. A. *J. Org. Chem.* **2009**, *74*, 4490–4498.
15. Guerra, W. D.; Rossi, R. A.; Pierini, A. B.; Barolo, S. M. *J. Org. Chem.* **2015**, *80*, 928–941.
16. Laha, J. K.; Barolo, S. M.; Rossi, R. A.; Cuny, G. D. *J. Org. Chem.* **2011**, *76*, 6421–6425.
17. Vaillard, V. A.; Budén, M. E.; Martín, S. E.; Rossi, R. A. *Tetrahedron Lett.* **2009**, *50*, 3829–3832.
18. Barolo, S. M.; Wang, Y.; Rossi, R. A.; Cuny, G. D. *Tetrahedron* **2013**, *69*, 5487–5494.
19. Guerra, W. D.; Rossi, R. A.; Pierini, A. B.; Barolo, S. M. *J. Org. Chem.* **2016**, *81*, 4965–4973.
20. Han, Y.-Y.; Wang, H.; Yu, S. *Org. Chem. Front.* **2016**, *3*, 953–956.
21. Guastavino, J. F.; Rossi, R. A. *J. Org. Chem.* **2012**, *77*, 460–472.
22. Peisino, L. E.; Camargo Solorzano, G. P.; Budén, M. E.; Pierini, A. B. *RSC Adv.* **2015**, *5*, 36374–36384.
23. (a) Schmidt, L. C.; Argüello, J. E.; Peñéñory, A. B. *J. Org. Chem.* **2007**, *72*, 2936–2944; (b) Budén, M. E.; Guastavino, J. F.; Rossi, R. A. *Org. Lett.* **2013**, *15*, 1174–1177.
24. Peñéñory, A. B.; Rossi, R. A. *Gazz. Chim. Ital.* **1995**, *125*, 605–609.
25. See Supplementary data.
26. Demas, J. N.; Crosby, G. A. *J. Phys. Chem.* **1971**, *75*, 991–1024.
27. Dewey, T. J. *Biophysical and Biochemical Aspects of Fluorescence Spectroscopy*; Plenum: New York, 1991; pp 1–41.
28. (a) Frei, R.; Wodrich, M. D.; Hari, D. P.; Borin, P.-A.; Chauvier, C.; Waser, J. *J. Am. Chem. Soc.* **2014**, *136*, 16563–16573; (b) Zhao, Y.; Truhlar, D. G. *Theor. Chem. Acc.* **2008**, *120*, 215–241; (c) Zhao, Y.; Truhlar, D. G. *Acc. Chem. Res.* **2008**, *41*, 157–167.
29. (a) Miertus, S.; Scrocco, E.; Tomasi, J. *Chem. Phys.* **1981**, *55*, 117–129; (b) Miertus, S.; Tomasi, J. *Chem. Phys.* **1982**, *65*, 239–245; (c) Cossi, M.; Barone, V.; Cammi, R.; Tomasi, J. *Chem. Phys. Lett.* **1996**, *255*, 327–335.
30. Marcus, R. A. *J. Chem. Phys.* **1965**, *43*, 679–701.
31. Using Marcus-Hush theory. See Eq. 3 and Ref. 30.
32. We carried out the reaction in the presence of DMSO-d_6 and we observed that deuterated reduced product, confirming that hydrogen-abstraction reaction is between DMSO and phenyl radical intermediate.
33. Argüello, J. E.; Peñéñory, A. B.; Rossi, R. A. *J. Org. Chem.* **2000**, *65*, 7175–7182.
34. This shorter wavelength was found to be more reductive due to the fact that a higher proportion of reduced product was found for **1a**. Even precursor **1c** afforded traces of corresponding reduced product, previously not found. This more reductive wavelength probably is leading intersystem crossing between single excited state to triplet state.
35. Goldstein, S.; Rabani, J. *J. Photochem. Photobiol., A* **2008**, *193*, 50–55.
36. Pan, X.; Wilcox, C. S. *J. Org. Chem.* **2010**, *75*, 6445–6451.
37. Bu, M.-J.; Lu, G.-P.; Cai, C. *Org. Chem. Front.* **2013**, 1–3.
38. Kim, B. S.; Lee, S. Y.; Youn, S. W. *Chem.—Asian. J.* **2011**, *6*, 1952–1957.
39. Zuo, Z.; Liu, J.; Nan, J.; Fan, L.; Sun, W.; Wang, Y.; Luan, X. *Angew. Chem., Int. Ed.* **2015**, *54*, 15385–15389.